Understanding the Electrolyte Background for Biochemical Sensing with Ion-Sensitive Field-Effect Transistors

Alexey Tarasov,[†,*] Mathias Wipf,[†] Ralph L. Stoop,[†] Kristine Bedner,[‡] Wangyang Fu,[†] Vitaliy A. Guzenko,[‡] Oren Knopfmacher,[†,§] Michel Calame,[†] and Christian Schönenberger[†]

[†]Department of Physics, University of Basel, Basel, Switzerland and [‡]Laboratory for Micro- and Nanotechnology, Paul Scherrer Institut, Villigen, Switzerland. [§]Present address: Department of Chemical Engineering, Stanford University, Stanford, California.

ABSTRACT

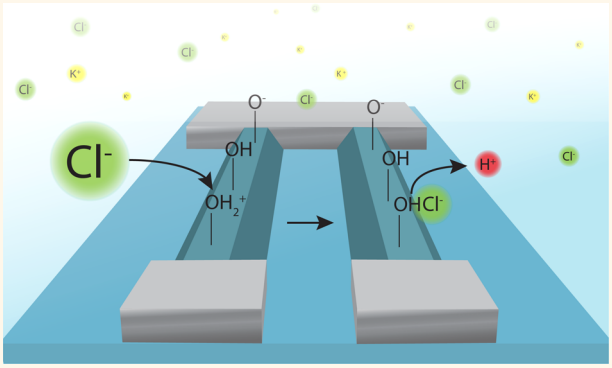

Silicon nanowire field-effect transistors have attracted substantial interest for various biochemical sensing applications, yet there remains uncertainty concerning their response to changes in the supporting electrolyte concentration. In this study, we use silicon nanowires coated with highly pH-sensitive hafnium oxide (HfO_2) and aluminum oxide (Al_2O_3) to determine their response to variations in KCl concentration at several constant pH values. We observe a nonlinear sensor response as a function of ionic strength, which is independent of the pH value. Our results suggest that the signal is caused by the adsorption of anions (Cl^-) rather than cations (K^+) on both oxide surfaces. By comparing the data to three well-established models, we have found that none of those can explain the present data set. Finally, we propose a new model which gives excellent quantitative agreement with the data.

KEYWORDS: nanowire · sensing · anion adsorption · high-k oxide · ion-sensitive field-effect transistor

Over the past decades, interfaces between oxides and electrolytes have received considerable attention in different scientific communities. In particular, the adsorption of inorganic salt ions on colloidal oxide surfaces has been extensively studied[1−6] and reviewed.[7,8] The adsorption mechanism was explained within the site-binding model (SBM)[9−11] by the surface complexation of ions at oppositely charged oxide sites. Apart from colloid science, a description of the oxide/electrolyte interface has been essential for the development of glass electrodes (GE). Recently, researchers celebrated the centenary of GEs and the related Nikolsky's ion exchange theory, which is widely used to describe not only GEs but also other ion-sensitive electrodes.[12−14] In the 1970s, the ion-sensitive field-effect transistors (ISFETs) emerged, combining the properties of a transistor with a GE-like interface.[15] Nikolsky's theory was quite naturally used to explain the experimental results obtained with ISFETs.[16,17] However, the Nikolsky−Eisenman equation is semiempirical, and its use is limited to estimating the selectivity of a sensor against interfering ions. To give a more detailed theoretical explanation, the successful SBM was later adapted to ISFETs[18,19] and simplified in the following years by Bergveld and co-workers.[20−23] With the rise of nanoscaled ISFETs,[24−27] the attention has again been drawn to the interactions between the active oxide surface and the ions in the electrolyte. Even though many pH measurements with nanowire-based ISFETs have been reported, for example,[28−30] surprisingly few attempts to measure changes in electrolyte concentration with miniaturized ISFETs have been published so far, with inconsistent results.[31−35] More specifically, Nikolaides *et al.*[32] and Park *et al.*[31] reported a weak nonlinear response of a SiO_2-coated FET to KCl or NaCl. In contrast, Clément *et al.* claimed a full linear Nernstian response of around 60 mV/dec to NaCl, using SiO_2-coated nanowire ISFETs. Unfortunately, none of these studies has performed a quantitative assessment of the data using a theoretical model. Recently, Zafar and co-workers[35] measured HfO_2-covered Si nanowires and did not observe any appreciable response up to 1 M NaCl. In our previous paper,[36] we showed that a minituarized

* Address correspondence to alexey.tarasov@unibas.ch.

Received for review August 20, 2012 and accepted September 27, 2012.

Published online September 27, 2012
10.1021/nn303795r

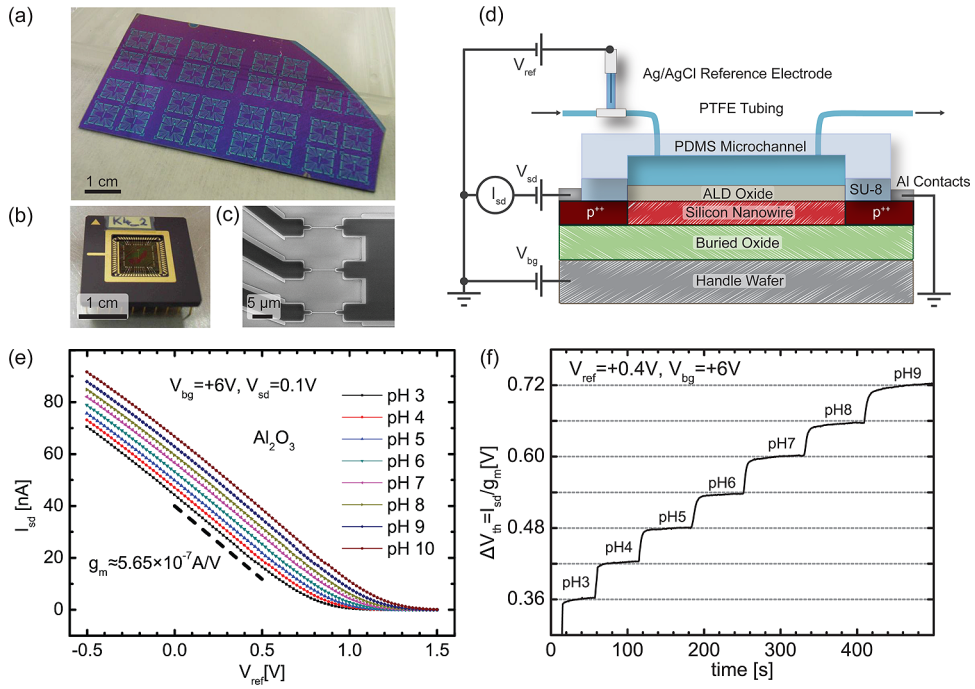

Figure 1. (a) Optical image of a wafer piece after electron beam lithography of the nanowires. The samples are arranged in 2 × 2 squares. Each sample consists of 48 nanowire FETs. Light areas are the nanowires and contact leads, dark areas are the buried oxide. (b) Sample after bonding into a chip carrier. (c) SEM image of three nanowires (thin horizontal lines) with contact areas on the left (source) and a common bus line on the right (drain). (d) Cross section of the fabricated device and a sketch of the measurement setup (not to scale). The liquid is delivered to the custom-made PDMS microchannels by a pump (indicated by arrows). A flow-through Ag/AgCl reference electrode is integrated in the Teflon (PTFE) tubing close to the microchannel. The working point of the nanowire transistor is adjusted by two voltages: a back-gate voltage V_{bg} (applied to the handle wafer) and a liquid gate voltage V_{ref} (applied to the reference electrode). A constant source−drain voltage V_{sd} = 0.1 V drives the source−drain current through the nanowire channel I_{sd}. (e) Nanowires are first characterized by transfer curves $I_{sd}(V_{ref})$ at different pH values of the buffer solution. The curves shift linearly to more positive V_{ref} values with increasing pH (see Figure 2b). The transconductance $g_m = \partial I_{sd}/\partial V_{ref}$ can be extracted from the linear region. (f) In addition, time-resolved pH measurements I_{sd}(time) were made. The measured I_{sd} was divided by g_m to obtain the threshold voltage shifts ΔV_{th}. The step height is close to the Nernst limit (58.2 mV/pH at 20 °C, indicated by horizontal grid lines). The time scale for the jumps is given by the liquid exchange rate.

ISFET with an Al_2O_3 interface only weakly responds to various types of ions up to a moderate concentration of 10 mM, at a constant pH ≈ 6. The results of both studies[35,36] were qualitatively described by the Bergveld model.[23]

In this work, we significantly expand our recent study by using silicon nanowires coated with high-k HfO_2 and Al_2O_3 to systematically measure their response to changes in KCl concentration up to 1 M, at several constant pH values. We observe a nonlinear behavior, which—unexpectedly—does not depend on the solution pH. We then compare the results with three different models, derived for conventional ISFETs or GEs, and conclude that none of those can satisfactorily describe the experimental data, mainly because a pH-dependent response to electrolyte ions is anticipated by all models. We propose a new adsorption model instead, which gives excellent quantitative agreement with the data.

RESULTS AND DISCUSSION

The samples were produced using a top-down approach according to the previously published protocol.[37] An optical image of a silicon-on-insulator (SOI) wafer part after electron beam lithography is shown in Figure 1a. The samples are arranged in 2 × 2 squares. After finishing the fabrication process, the wafer was cut and each sample was glued and wire-bonded into a chip carrier (Figure 1b). The sample comprises 48 nanowires of 8 different widths (100−1000 nm) but of the same length (6 μm) and height (80 nm). Figure 1c shows an SEM image of three individual nanowires (thin horizontal lines) with the respective contact areas on the left and a shared bus line on the right side (dark areas). A cross section of the final device including the measurement setup is schematically sketched in part d of Figure 1 (not to scale). To characterize the nanowires as pH sensors, two different types of measurements were performed. First, transfer curves $I_{sd}(V_{ref})$ of an Al_2O_3-coated sample at different pH values were recorded (Figure 1e). The curves shift to more positive gate values with increasing pH. The maximum possible response is given by the Nernst limit of $\ln(10)kT/e \approx 58.2$ mV/pH at 20 °C, where k is the Boltzmann constant, T the absolute temperature, and e the elementary charge. We will analyze the shifts in the

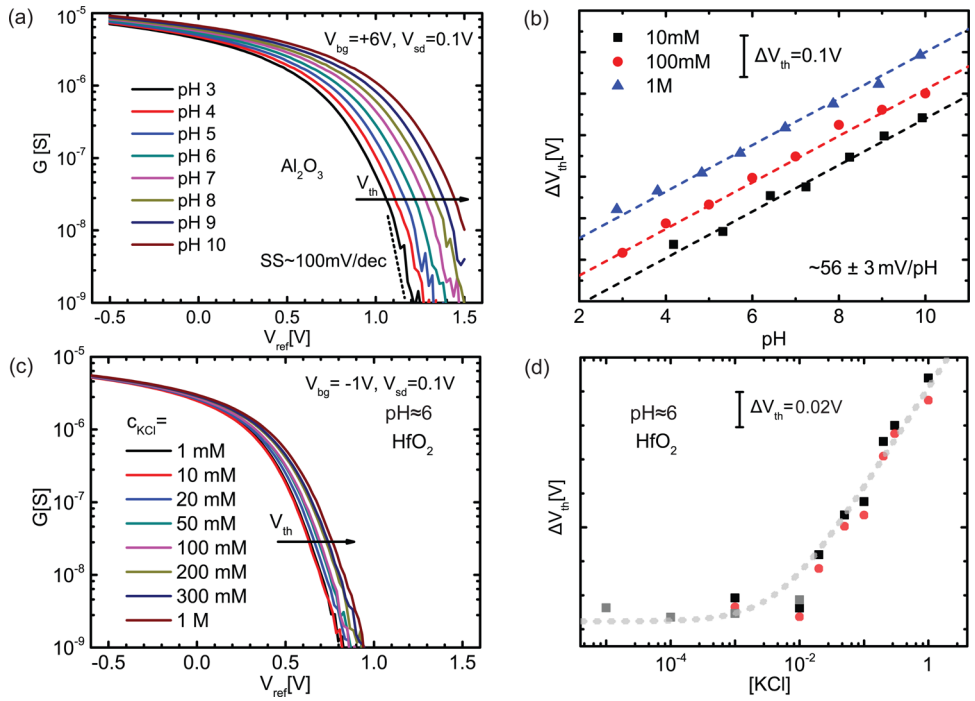

Figure 2. (a) Conductance *G vs* V_{ref} for an Al_2O_3-coated nanowire on a semilog plot (same data as in Figure 1e). The subthreshold swing SS is around 100 mV/dec. The pH response is quantified by the shift of the threshold voltage V_{th} upon a change in pH. We read out the threshold voltage V_{th} as a value of V_{ref} at a constant G = 20 nS (along the arrow). The threshold voltage shift ΔV_{th} as a function of pH is shown in (c) for three different ionic strengths of the electrolyte. ΔV_{th} is a linear function of pH with the slope of ~56 mV/pH (indicated by dashed lines). No significant dependence of the slope on the ionic strength is found. (c) Transfer curve of a HfO_2-coated nanowire for different concentrations of the electrolyte ≥1 mM but at a constant pH ≈6. V_{th} shifts to more positive values with increasing ionic strength. This indicates the adsorption of negatively charged ions (chloride). (d) Threshold shift ΔV_{th} *vs* KCl concentration read out from the measurement shown in c (dark squares), from a different measurement with the same wire (light squares), and from a different nanowire with nominally the same dimensions (circles). A nonlinear behavior is observed. The dashed line is a guide to the eye.

next paragraph. The transconductance $g_m = \partial I_{sd}/\partial V_{ref}$ can be extracted from the linear region and is nearly constant for all pH values. Alternatively, the source–drain current I_{sd} can be measured as a function of time (Figure 1f). The transconductance value from Figure 1e is used to compute the threshold voltage shift $\Delta V_{th} = I_{sd}/g_m$. Clear signal steps are observed as the solution is exchanged. In the presented example, the time scale for the jump is given by the liquid exchange rate and not by the transistor. Sensor response times below 200 ms were easily reached. The step height is close to 60 mV/pH, as indicated by horizontal grid lines.

In this paragraph, we will analyze the transfer curves more carefully. To do so, we plot the data shown in Figure 1e as conductance *G versus* V_{ref} on a semilog plot (Figure 2a). The subthreshold swing SS is around 100 mV/dec (dashed line). To quantify the shifts of the transfer curve, we read out the threshold voltage V_{th} as the value of V_{ref} at a constant conductance G = 20 nS (along the arrow). Then, we plot V_{th} as a function of pH for three different total ionic strengths of the electrolyte (Figure 2b). The threshold voltage shifts linearly with pH, exhibiting a nearly Nernstian response of ~56 mV/pH (dashed lines). These relative shifts ΔV_{th} are independent of the ionic strength. Similar results were obtained with a HfO_2-coated sample. In Figure 2c, the concentration of KCl in deionized water is varied (HfO_2 sample). The pH value of all solutions was ≈6. The curves shift to more positive gate values with increasing ionic strength. In contrast to the pH measurement, the V_{th} shift to salt is nonlinear (see Figure 2d). Up to 10 mM, almost no shift occurs, as we have already reported.[36] Above this value, the nanowire starts responding strongly to the changes in ionic strength (up to full Nernstian response). Because V_{th} shifts toward more positive values, we conclude that the effect must be due to the adsorption of negative ions, that is chloride Cl^-. Very similar behavior has been observed using different salts, in particular, $NaNO_3$ and Na_2SO_4 (see Supporting Information). In the following, we focus on potassium chloride as a representative example. Moreover, this effect does not show any significant pH dependence and is very similar for both HfO_2 and Al_2O_3 interfaces, as we will see. In addition, no significant dependence of the effect on the nanowire width is found (see Supporting Information).

In Figure 3a–c, the experimental results for a HfO_2-coated sample (solid symbols) are compared with three existing models (lines). Note that on the horizontal axis, the KCl concentration c_{KCl} was replaced by the activity a_{Cl^-}, which was estimated using the specific

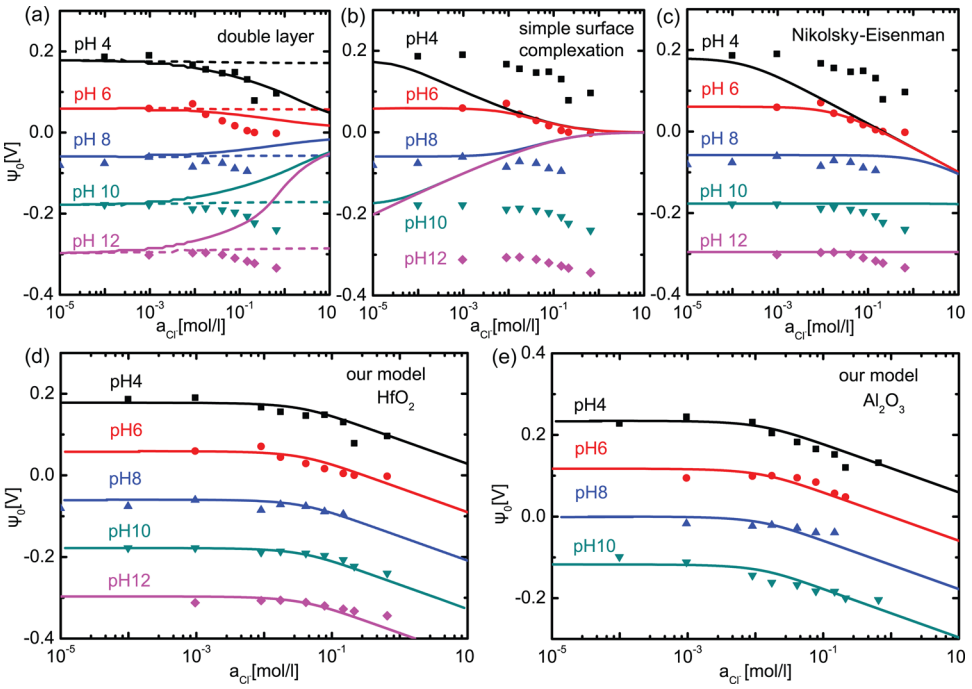

Figure 3. Plots of the surface potential ψ_0 *versus* the activity of the chloride ions in the bulk solution a_{Cl^-}. Solid symbols represent experimental data points for a HfO_2-coated (a–d) and an Al_2O_3-coated sample (e), whereas lines are theoretical fits based on different models. The measured threshold voltages V_{th} were converted to surface potential *via* $\psi_0 = V_{th}(PZC) - V_{th}$. The point of zero charge is set to PZC = 7 for HfO_2 (a–d) and PZC = 8 for Al_2O_3 (e). We observe that the measured data points move to more negative ψ_0 with increasing a_{Cl^-}, irrespective of the pH value. This implies the adsorption of negatively charged species on the surface. (a) Fits of the simple site-binding model with parameters from literature (dashed lines) and the best fitting parameters (solid lines). In this model, the ionic strength changes the surface potential *via* the double-layer capacitance. In (b), the electrolyte ions contribute to ψ_0 by a complexation reaction with the oppositely charged surface groups. (c) Fits of the well-known Nikolsky–Eisenman equation. The only changing parameter from curve to curve is the proton activity. All other parameters are fixed, unlike previous works. (d) In contrast to the fits shown in (a–c), our model describes the complete data set for all pH values. (e) Similarly good agreement between experiment and model was achieved for an Al_2O_3-coated sample.

ion interaction theory (SIT); see, for example, ref 39. This correction is needed because the approximation $c_{KCl} \approx a_{Cl^-}$ is no longer valid at high ionic strength due to interaction between the electrolyte ions. On the vertical axis, the measured threshold voltages V_{th} were converted to surface potential *via* $\psi_0 = V_{th}(PZC) - V_{th}$, where $V_{th}(PZC)$ is the threshold voltage at the assumed point of zero charge (PZC). On the basis of previously published studies, we have chosen PZC = 7 for HfO_2 (Figure 3 a–d)[40] and PZC = 8 for Al_2O_3 (e).[8,30] The resulting ψ_0 is zero at pH = PZC, positive at pH < PZC, and negative at pH > PZC. We observe that the measured data points move to more negative ψ_0 with increasing KCl concentration, irrespective of the pH value. As mentioned before, this indicates the adsorption of negatively charged species.

The most obvious model to start with is the site-binding model, which has become a standard for describing ISFET response to ions. In Figure 3a, fits of a simple SBM are shown, in which the surface potential is determined by protonation or deprotonation of the amphoteric surface groups MOH:

$$MOH \rightleftharpoons MO^- + H_s^+, K_a = \frac{\nu_{MO^-} a_{H_s^+}}{\nu_{MOH}} \qquad (1)$$

$$MOH_2^+ \rightleftharpoons MOH + H_s^+, K_b = \frac{\nu_{MOH} a_{H_s^+}}{\nu_{MOH_2^+}} \qquad (2)$$

where M denotes a metal, H_s^+ a surface proton, ν the number of particular sites, $a_{H_s^+}$ the activity of surface protons, and K_a and K_b the dissociation and association constant, respectively. On the basis of these reactions, the response to pH can be described by an analytical expression $a_{H^+}(\psi_0)$ with two key parameters: the surface buffer capacitance C_s and the double-layer capacitance C_{dl}. A detailed derivation of the SBM can be found in our previous study[37] or in the original works.[9,18] The buffer capacitance is the ability of the surface to give away or take up protons which is determined by the density of active surface sites (OH groups). The higher the C_s, the more linear and closer to the Nernstian value is the pH response. In this approach, the electrolyte ions can influence the potential *via* the Debye screening length, which enters the double-layer capacitance $C_{dl} = C_{dif}C_{st}/(C_{dif} + C_{st})$, where C_{st} is the constant Stern layer capacitance and C_{dif} is the differential capacitance, mainly determined by the ionic strength. However, the influence is very small (dashed lines) if literature values for $C_{st} = 0.2$ F/m^{-2} and the number of active sites $N_s = 10^{19}$m^{-2} are taken.[18,19,30,37]

Especially, C_{st} proves to be the limiting factor because it leads to saturation of C_{dl} at ≈0.16 F/m^{-2}. If we increase C_{st} to 20 F/m^{-2} and reduce N_s somewhat to 4 × 10^{18}m^{-2}, the influence of ionic strength can become pronounced (solid lines). However, as only the data at pH 4 can be fitted nicely, two major difficulties of this model become obvious. First, the SBM predicts a sign change of the effect; that is, the curves bend downward if pH < PZC and upward if pH > PZC. In other words, if the surface is, for instance, positively charged (pH 4 and 6), only negative ions are attracted, neutralizing the surface charge. Analogously, a negative surface (pH 8, 10, 12) attracts positively charged electrolyte ions. The latter case was not observed in the experiment, despite covering a wide pH range. The second problem of the model is that the pH response (*i.e.*, the vertical separation between the five solid curves) gets smaller with increasing ionic strength. A fully Nernstian behavior only occurs at low activities $a_{Cl^-} < 10^{-3}$ mol/L, whereas at 1 M, for example, the model predicts a weak and nonlinear pH response of roughly 25 mV/pH. This also strongly disagrees with the experiment shown in Figure 2b, in which nearly ideal pH response was observed even at 1 M background concentration.

Another way of including the electrolyte ions in the SBM is by writing down two additional equations for the so-called surface complexation:

$$MOH_2^+ + Cl_s^- \rightleftharpoons MOH_2Cl, K_c = \frac{\nu_{MOH_2Cl}}{\nu_{MOH_2^+} a_{Cl_s^-}} \quad (3)$$

$$MO^- + K_s^+ \rightleftharpoons MOK, K_d = \frac{\nu_{MOK}}{\nu_{MO^-} a_{K_s^+}} \quad (4)$$

Combining the reactions (eq 1−eq 4), new analytical functions $a_{Cl^-}(\psi_0)$ and $a_{K^+}(\psi_0)$ can be derived. The best fits are shown in Figure 3b using the following parameters: $K_a = K_b = 10^{-7}$, $K_c = K_d = 5 \times 10^{-4}$, number of active surface sites $N_s = 10^{19}$ m^{-2}. The double-layer capacitance was set to a constant value $C_{dl} = 0.16$ F/m^2, as discussed before.[37] Like in the previous case, huge discrepancies appear between experiment and model. In fact, there is even a third difficulty: the activity at which the curves start to bend now depends on pH. This can be explained as follows: when the surface is strongly charged (far away from PZC), the equilibrium in eq 3 and eq 4 is shifted to the right side. Electrolyte ions are easily attracted and cause a significant effect on the surface potential. In contrast, when only few charged sites are available close to the PZC, a much higher ionic strength is needed to shift the equilibrium toward products and to neutralize the remaining sites.

Instead of the SBM, Nikolsky's ion exchange theory is often used to describe the basic chemistry at the surface of a (glass) electrode, with the most prominent example being as follows:

$$H_s^+ + Na_b^+ \rightleftharpoons H_b^+ + Na_s^+, \ln K = \ln \frac{a_{H_b^+} a_{Na_s^+}}{a_{H_s^+} a_{Na_b^+}} \quad (5)$$

where K is the exchange constant, the subscript "b" denotes activities and ions in bulk solution, and "s" stands for surface. The semiempirical Nikolsky−Eisenman equation can then be derived, which is often used to determine the selectivity of an ion-sensitive electrode to an interfering ion B with respect to the primary ion A:

$$V = \text{constant} + \frac{RT}{F} \ln(a_A + K a_B) \quad (6)$$

where V is the measured voltage, R the gas constant, T the absolute temperature, F the Faraday constant, a_A the activity of the primary ion (here, A = Cl$^-$), a_B the activity of the interfering ion (B = OH$^-$), and K is the exchange constant. The best fits can be found in Figure 3c. All curves share the same set of parameters, except for the proton activity. The proton activity has a two-fold impact on the fitted curves: first, it determines the vertical position of the flat part relative to PZC; and second, it fixes the position at which the transition from the flat to the linear part takes place. Again, only the data at pH 6 is described well by the model. The only way to fit the whole data set is to let the constant K act as a free fitting parameter. This would compensate the shift of the transition point caused by the proton activity, as mentioned before. This is a popular approach, the "constant" K is often called "selectivity coefficient", which depends on the pH value and is treated as a free fitting parameter (see, for example, refs 17 and 34). The fact that K has to be adjusted with respect to pH indicates that K is ill-defined as a reaction constant. Interestingly, we found that $K/a_{pH} \approx$ constant. In other words, if the proton activity is changed by a factor of 10 (ΔpH = 1), K has to be changed by 10 times as well to keep the same quality of the fitting. Treating the constant K as a free fitting parameter might optimize the fits to the data and provide some numbers for the selectivity, but it is not satisfactory from the physical point of view.

On the basis of the above considerations, we have decided to modify the site-binding model to better fit the whole data set. We found that a slight change of the reaction equation leads to an excellent agreement between experiment and model for both HfO_2 (Figure 3d) and Al_2O_3 (Figure 3e). The assumed adsorption mechanism can be described as surface complexation of the following type:

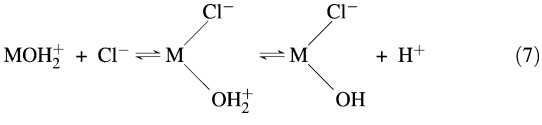

(7)

This mechanism is not limited to the adsorption of Cl$^-$ and can also be applied to other anions (see Supporting Information). A review of possible anion chemisorption mechanisms on hydroxylated metal oxide surfaces is available in ref 38. Rewriting eq 7 in a more

compact way yields the new reaction equation, in addition to eq 1 and eq 2:

$$MOH_2^+ + Cl_s^- \rightleftharpoons MOHCl^- + H_b^+, K_c' = \frac{\nu_{MOHCl^-} a_{H_b^+}}{\nu_{MOH_2^+} a_{Cl_s^-}} \quad (8)$$

with K_c' being a real reaction constant (*i.e.*, pH-independent). We deduced a value of $K_c' \approx 3.3 \times 10^{-6}$ from the fits. The remaining parameters were set as follows: $K_a = K_b = 10^{-7}$, $N_s = 10^{19}$ m^{-2}, $C_{dl} = 0.16$ F/m^2. The value for the number of sites N_s is taken from literature and corresponds to the upper limit for oxide surfaces, given by bonding distances in oxides (see ref 41). Reducing this number would affect the fitted curves in Figure 3d,e in the following way: the vertical separation between the curves would decrease and become nonlinear because the ideal pH response would no longer be described by the model. As a consequence, the decreased pH response would immediately contradict the pH measurements in Figures 1 and 2. We have discussed the influence of N_s as well as K_a and K_b on the pH sensitivity in our recent publication.[37]

Equation 8 implies that a chloride ion from the solution forms a complex with the surface hydroxyl groups and replaces a proton at the surface, which goes to the bulk solution. We emphasize that the proton has to leave the surface for an appropriate description of the surface potential. This interesting insight can be further supported by recent molecular dynamics simulations of an oxide/electrolyte interface similar to ours.[42] In particular, the authors showed that the first water layers organize on the surface of oxidized aluminum *via* hydrogen bonding (see also ref 38). If NaCl solution was added to the model, the first monolayer of water was disturbed by the electrolyte. Chloride ions displaced water molecules that were originally bound to the surface. As a result, Cl^- adsorbed on the oxide building a surface complex with the hydroxyl groups. The attractive interaction (O−)H···Cl^- can reasonably be described as hydrogen bonds.[43] In contrast, the alkali ions did not displace any adsorbed surface waters and stayed at a larger distance to the surface.

CONCLUSIONS

To conclude, we have studied the response of HfO_2- and Al_2O_3-coated silicon nanowire field-effect sensors to KCl at several pH values. A significant signal change is observed only at high ionic strengths, >10 mM, with both oxides behaving very similarly. Our measurements indicate that only anions are adsorbed on the surface, independent of the pH value. This result strongly contradicts the established site-binding model, which predicts that both types of ions can be adsorbed depending on the surface charge (or pH). Within the site-binding model, neither a double-layer effect nor a simple surface complexation can explain our observations. Moreover, the widely used Nikolsky−Eisenman equation cannot satisfactorily describe the data in a physically meaningful way. We suggest a new model instead, which gives excellent quantitative agreement with the experimental data. According to our model, the anions directly interact with the hydroxyl surface groups and replace previously adsorbed protons from the surface. Recently published molecular dynamics simulations further support our model.[42]

In our opinion, these results are relevant for any type of biochemical sensing applications where the electrolyte concentration might vary, for instance, due to some biological processes. The background effects of the electrolyte ions have to be understood and clearly separated from the signals caused by the actual analyte. Even slight changes of the ionic strength in the physiological range can cause a significant sensor response. Therefore, the pH changes and ionic strength variations should be always monitored in parallel to any other specific detection experiments. We underline the importance of differential measurements for reliable sensing results. If different specific functionalizations are used on one chip, nanowire arrays represent an ideal platform for such multianalyte detection systems.

METHODS

Device Fabrication. The samples were produced from bonded silicon-on-insulator (SOI) wafers (Soitec, France) in a top-down approach according to the previously published protocol.[37] The wafer has a 85 nm thick p-Si (100) device layer with a resistivity of 8.5−11.5 Ωcm and a 145 nm thick buried SiO_2 layer (BOX). As a first step, a 15 nm thin thermal SiO_2 was grown on the Si device layer. The nanowire pattern was defined by electron beam lithography (EBL) and transferred to the 15 nm SiO_2 by dry etching. The shaped oxide acted as a mask for the wet chemical etching of the Si device layer using a solution of tetramethylammonium hydroxide (TMAH) and isopropyl alcohol at 45 °C (9:1 volume ratio). The lithographic dimensions of the NW were as follows: width = 100−1000 nm, length = 6 μm, height = 80 nm. The source and drain contact areas were heavily doped by BF_2^+ ions (energy = 33 keV, dose = 2.3×10^{15} cm^{-2}). The ion implantation step was followed by thermal annealing in a forming gas (6 min at 950 °C) to activate the dopants. The ohmic contacts were completed by Al−Si(1%) metallization and annealing at 450 °C. To reduce leakage currents in a liquid environment and to optimize the pH response, the samples were coated by a thin layer of a high-quality Al_2O_3 or HfO_2 (10−20 nm; atomic layer deposition (ALD) at 225 °C, Savannah S100, Cambridge NanoTech). The packaging for the operation in an electrolyte environment included a micrometer-sized liquid channel, lithographically shaped in a 2 μm thick photoresist (SU-8 2002, MicroChem), wire-bonding into a chip carrier, and epoxy sealing of the contacts (Epotek 302-3M, Epoxy Technology).

Preparation of Electrolyte Solutions. Standard pH buffer solutions were used for the pH measurements (Titrisol, Merck). For measurements in KCl solutions, potassium chloride salt (ACS grade, 99.0−100.5%, Alfa Aesar) was dissolved in deionized

water (resistivity = 17 MΩcm). The pH of the solutions was adjusted by adding small concentrations (1−2 mM) of CH_3COOH (pH 4), NH_3 (pH 8), KOH (pH 10), and 5−10 mM KOH (pH 12). Without an additional agent, the pH of the KCl solutions stayed around 6. The pH values of all solutions were monitored by a glass electrode (691 pH Meter, Metrohm).

Electrical Measurements in Liquid. The samples were cleaned by UV/ozone treatment (20 min) before the measurements. Then, a polydimethylsiloxane (PDMS) stamp with custom-made microchannels was placed on the chip, and the first solution was pumped through by a tubing pump (MCP, Ismatec). Polytetrafluorethylen (PTFE, Teflon) tubes were used to access the microchannels. A flow-through Ag/AgCl reference electrode (Microelectrodes, Inc.) was immersed in the tubing close to the microchannels to control the liquid potential. The samples were left for 2 h in contact with the solution to stabilize the oxide/electrolyte interface. After that, a nanowire conductance map was measured by a source-meter (Keithley 2636A) as a function of both back-gate V_{bg} and the liquid potential V_{ref} (dual-gate approach[29,44,45]) at constant source−drain voltage V_{sd} = 100 mV. Using a switching box (Keithley 3706), up to 48 NWs were measured in the same experiment to have some statistics and to study the size dependence. As soon as such a conductance map was obtained, the electrolyte solution was exchanged using a low-pressure valve selector (VICI Cheminert, Valco Instruments Co. Inc.) and a pump. Again, a map was measured after 30 min of stabilization time. All devices were automatically controlled by a self-made LabView program.

Conflict of Interest: The authors declare no competing financial interest.

Acknowledgment. The authors gratefully acknowledge the support by the Swiss Nanoscience Institute (SNI), the Swiss Nano-Tera program, Sensirion AG, and the European Commission under the FP7-NMP project Hysens (263091).

Supporting Information Available: Measurements in KCl for different nanowire widths; results obtained using other salts, such as $NaNO_3$ and Na_2SO_4. This material is available free of charge *via* the Internet at http://pubs.acs.org.

REFERENCES AND NOTES

1. Modi, H. J.; Fuerstenau, D. W. Streaming Potential Studies on Corundum in Aqueous Solutions of Inorganic Electrolytes. *J. Phys. Chem.* **1957**, *61*, 640–643.
2. Hunter, R. J.; Wright, H. J. L. The Dependence of Electrokinetic Potential on Concentration of Electrolyte. *J. Colloid Interface Sci.* **1971**, *37*, 564–580.
3. Huang, C.-P.; Stumm, W. Specific Adsorption of Cations on Hydrous γ-Al_2O_3. *J. Colloid Interface Sci.* **1973**, *43*, 409–420.
4. Sprycha, R. Electrical Double Layer at Alumina/Electrolyte Interface. *J. Colloid Interface Sci.* **1989**, *127*, 1–11.
5. Johnson, S. B.; Scales, P. J.; Healy, T. W. The Binding of Monovalent Electrolyte Ions on α-Alumina. I. Electroacoustic Studies at High Electrolyte Concentrations. *Langmuir* **1999**, *15*, 2836–2843.
6. Kosmulski, M. Confirmation of the Differentiating Effect of Small Cations in the Shift of the Isoelectric Point of Oxides at High Ionic Strengths. *Langmuir* **2002**, *18*, 785–787.
7. Hunter, R. J. *Zeta Potential in Colloid Science: Principles and Applications*, 2nd ed.; Academic Press: London, 1988.
8. Kosmulski, M. Compilation of PZC and IEP of Sparingly Soluble Metal Oxides and Hydroxides from Literature. *Adv. Colloid Interface Sci.* **2009**, *152*, 14–25.
9. Yates, D. E.; Levine, S.; Healy, T. W. Site-Binding Model of the Electrical Double Layer at the Oxide/Water Interface. *J. Chem. Soc., Faraday Trans.* **1974**, *70*, 1807–1818.
10. Healy, T. W.; White, L. R. Ionizable Surface Group Models of Aqueous Interfaces. *Adv. Colloid Interface Sci.* **1978**, *9*, 303–345.
11. Davis, J. A.; James, R. O.; Leckie, J. O. Surface Ionization and Complexation at the Oxide/Water Interface I. Computation of Electrical Double Layer Properties in Simple Electrolytes. *J. Colloid Interface Sci.* **1978**, *63*, 480–499.
12. Baucke, F. G. K. Fundamental and Applied Electrochemistry at an Industrial Glass Laboratory—An Overview. *J. Solid State Electrochem.* **2011**, *15*, 23–46.
13. Belyustin, A. A. The Centenary of Glass Electrode: From Max Cremer to F. G. K. Baucke. *J. Solid State Electrochem.* **2011**, *15*, 47–65.
14. Scholz, P. Nikolsky's Ion Exchange Theory *versus* Baucke's Dissociation Mechanism of the Glass Electrode. *J. Solid State Electrochem.* **2011**, *15*, 23–46.
15. Bergveld, P. Development of an Ion-Sensitive Solid-State Device for Neuro-Physiological Measurements. *IEEE Trans. Biomed. Eng.* **1970**, *BME-17*, 70–71.
16. Bergveld, P. Development, Operation, and Application of the Ion-Sensitive Field-Effect Transistor as a Tool for Electrophysiology. *IEEE Trans. Biomed. Eng.* **1972**, *BME-19*, 342–351.
17. Sobczynska, D.; Torbicz, W. ZrO_2 Gate pH-Sensitive Field Effect Transistor. *Sens. Actuators* **1984**, *6*, 93–105.
18. Bousse, L.; de Rooij, N. F.; Bergveld, P. Operation of Chemically Sensitive Field-Effect Sensors as a Function of the Insulator-Electrolyte Interface. *IEEE Trans. Electron Devices* **1983**, *ED-30*, 1263–1270.
19. Fung, C. D.; Cheung, P. W.; Ko, W. H. A Generalized Theory of an Electrolyte-Insulator-Semiconductor Field-Effect Transistor. *IEEE Trans. Electron Devices* **1986**, *ED-33*, 8–18.
20. van Hal, R. E. G.; Eijkel, J. C. T.; Bergveld, P. A Novel Description of ISFET Sensitivity with the Buffer Capacity and Double-Layer Capacitance as Key Parameters. *Sens. Actuators, B* **1995**, *24−25*, 201–205.
21. van Hal, R. E. G.; Eijkel, J. C. T.; Bergveld, P. A General Model To Describe the Electrostatic Potential at Electrolyte Oxide Interfaces. *Adv. Colloid Interface Sci.* **1996**, *69*, 31–62.
22. van Kerkhof, J. C.; Eijkel, J. C. T.; Bergveld, P. ISFET Responses on a Stepwise Change in Electrolyte Concentration at Constant pH. *Sens. Actuators, B* **1994**, *18−19*, 56–59.
23. Bergveld, P. Thirty Years of ISFETOLOGY—What Happened in the Past 30 Years and What May Happen in the Next Thirty Years. *Sens. Actuators, B* **2003**, *88*, 1–20.
24. Zacharias, M.; Ramgir, N. S.; Yang, Y. Nanowire-Based Sensors. *Small* **2010**, *6*, 1705–1722.
25. Kolmakov, A.; Moskovits, M. Chemical Sensing and Catalysis by One-Dimensional Metal-Oxide Nanostructures. *Annu. Rev. Mater. Res.* **2004**, *34*, 151–180.
26. Kwon, Y. K.; Lee, M; Baik, K. Y.; Noah, M.; Lee, J. O.; Hong, S. Nanowire and Nanotube Transistors for Lab-on-a-Chip Applications. *Lab Chip* **2009**, *9*, 2267–2280.
27. Lieber, C. M.; Patolsky, F.; Zheng, G. F. Nanowire-Based Biosensors. *Anal. Chem.* **2006**, *78*, 4260–4269.
28. Cui, Y. Q.; Wei, Q.; Park, H. K.; Lieber, C. M. Nanowire Nanosensors for Highly Sensitive and Selective Detection of Biological and Chemical Species. *Science* **2001**, *293*, 1289–1292.
29. Knopfmacher, O.; Tarasov, A.; Fu, W.; Wipf, M.; Niesen, B.; Calame, M.; Schönenberger, C. Nernst Limit in Dual-Gated Si-Nanowire FET Sensors. *Nano Lett.* **2010**, *10*, 2268–2274.
30. Chen, S.; Bomer, J. G.; Carlen, E. T.; van den Berg, A. Al_2O_3/Silicon NanoISFET with Near Ideal Nernstian Response. *Nano Lett.* **2011**, *11*, 2334–2341.
31. Park, I.; Li, Z.; Pisano, A. P.; Williams, R. S. Top-Down Fabricated Silicon Nanowire Sensors for Real-Time Chemical Detection. *Nanotechnology* **2009**, *21*, 015501–015509.
32. Nikolaides, M. G.; Rauschenbach, S.; Luber, S.; Bucholz, K.; Tornow, M.; Abstreiter, G.; Bausch, A. R. Silicon-on-Insulator Based Thin-Film Resistor for Chemical and Biological Sensor Applications. *ChemPhysChem* **2003**, *4*, 1104–1106.
33. Clément, N.; Nishiguchi, K.; Dufreche, J. F.; Guerin, D.; Fujiwara, A.; Vuillaume, D. A Silicon Nanowire Ion-Sensitive Field-Effect Transistor with Elementary Charge Sensitivity. *Appl. Phys. Lett.* **2011**, *98*, 014104–014106.
34. Lu, T.-F.; Yang, C.-M.; Wang, J.-C.; Ho, K.-I.; Chin, C.-H.; Pijanowska, D.; Jaroszewicz, B.; Lai, C.-S. Characterization of K^+ and Na^+-Sensitive Membrane Fabricated by CF_4 Plasma Treatment on Hafnium Oxide Thin Films on ISFET. *J. Electrochem. Soc.* **2011**, *158*, J91–J95.

35. Zafar, S.; D'Emic, C.; Afzali, A.; Fletcher, B.; Zhu, Y.; Ning, T. Optimization of pH Sensing Using Silicon Nanowire Field Effect Transistors with HfO_2 as the Sensing Surface. *Nanotechnology* **2011**, *22*, 405501.
36. Knopfmacher, O.; Tarasov, A.; Wipf, M.; Fu, W.; Calame, M.; Schönenberger, C. Silicon-Based Ion-Sensitive Field-Effect Transistor Shows Negligible Dependence on Salt Concentration at Constant pH. *ChemPhysChem* **2012**, *13*, 1157–1160.
37. Tarasov, A.; Wipf, M.; Bedner, K.; Kurz, J.; Fu, W.; Guzenko, V. A.; Knopfmacher, O.; Stoop, R. L.; Calame, M.; Schönenberger, C. True Reference Electrode Realized with Silicon Nanowires. *Langmuir* **2012**, *28*, 9899–9905.
38. Blesa, M. A.; Weisz, A. D.; Morando, P. J.; Salfity, J. A.; Magaz, G. E.; Regazzoni, A. E. The Interaction of Metal Oxide Surfaces with Complexing Agents Dissolved in Water. *Coord. Chem. Rev.* **2000**, *196*, 31–63.
39. Bretti, C.; Foti, C.; Porcino, N.; Sammartano, S. SIT Parameters for 1:1 Electrolytes and Correlation with Pitzer Coefficients. *J. Solution Chem.* **2006**, *35*, 1401–1415.
40. Kosmulski, M. Attempt To Determine Pristine Points of Zero Charge of Nb_2O_5, Ta_2O_5, and HfO_2. *Langmuir* **1997**, *13*, 6315–6320.
41. van den Berg, A.; Bergveld, P; Reinhoudt, D. N.; Sudhölter, E. J. R. Sensitivity Control of ISFETs by Chemical Surface Modification. *Sens. Actuators* **1985**, *8*, 129–148.
42. Criscenti, L. J.; Cygan, R. T.; Kooser, A. S.; Moffat, H. K. Water and Halide Adsorption to Corrosion Surfaces: Molecular Simulations of Atmospheric Interactions with Aluminum Oxyhydroxide and Gold. *Chem. Mater.* **2008**, *20*, 4682–4693.
43. Taylor, R.; Kennard, O. Crystallographic Evidence for the Existence of C—H···O, C—H···N, and C—H···Cl Hydrogen Bonds. *J. Am. Chem. Soc.* **1982**, *104*, 5063–5070.
44. Knopfmacher, O.; Keller, D.; Calame, M.; Schönenberger, C. Dual Gated Silicon Nanowire Field Effect Transistors. *Procedia Chem.* **2009**, *1*, 678–681.
45. Tarasov, A.; Fu, W.; Knopfmacher, O.; Brunner, J.; Calame, M.; Schönenberger, C. Signal-to-Noise Ratio in Dual-Gated Silicon Nanoribbon Field-Effect Sensors. *Appl. Phys. Lett.* **2011**, *98*, 012114.